Carbohydrate Polymers 286 (2022) 119284

Contents lists available at ScienceDirect

Carbohydrate Polymers

journal homepage: www.elsevier.com/locate/carbpol

Alginate and tunicate nanocellulose composite microbeads – Preparation, characterization and cell encapsulation

Joachim S. Kjesbu [a], Daria Zaytseva-Zotova [a], Sanna Sämfors [b], Paul Gatenholm [b,c], Christofer Troedsson [d], Eric M. Thompson [d,e], Berit Løkensgard Strand [a,*]

[a] NOBIPOL, Department of Biotechnology and Food Science, Norwegian University of Science and Technology, N-7491 Trondheim, Norway
[b] Department of Chemistry and Chemical Engineering, Biopolymer Technology, Wallenberg Wood Science Center, Chalmers University of Technology, Gothenburg, Sweden
[c] CELLHEAL AS, Sandvika, Norway
[d] Ocean TuniCell AS, N-5258 Blomsterdalen, Norway
[e] Department of Biological Sciences, University of Bergen, N-5006 Bergen, Norway

ARTICLE INFO

Keywords:
Alginate
Cellulose nanofibrils
Tunicate
Microbeads
Cell encapsulation

ABSTRACT

Alginate has been used for decades for cell encapsulation. Cellulose nanofibrils (CNF) from tunicates are desirable in biomedicine due to high molecular weight, purity, crystallinity, and sustainable production. We prepared microbeads of 400–600 μm of alginate and tunicate CNF. Greater size, dispersity and aspect ratio were observed in microbeads with higher fractions of CNF. CNF content in Ca-crosslinked alginate microbeads decreased stability upon saline exposure, whereas crosslinking with calcium (50 mM) and barium (1 mM) yielded stable microbeads. The Young's moduli of gel cylinders decreased when exchanging alginate with CNF, and slightly increased permeability to dextran was observed in microbeads containing CNF. Encapsulation of MC3T3 cells revealed high cell viability after encapsulation (83.6 ± 0.4%) in beads of alginate and CNF. NHDFs showed lower viability but optimizing mixing and production techniques of microbeads increased cell viability (from 66.2 ± 5.3% to 72.7 ± 7.5%).

1. Introduction

Alginates are commonly used for cell encapsulation due to hydrogel formation in physiological conditions, resulting in high viability and function of the encapsulated cells. Alginate hydrogel microbeads can be produced by the extrusion of a viscous alginate solution through a needle with an electrostatic potential between the needle and cross-linking solution (Strand et al., 2002). Alginates are naturally occurring linear polysaccharides composed of 1,4-linked β-D-mannuronic acid (M) and α-L-guluronic acid (G) residues which are arranged into blocks of repeating M, G or MG. Alginates with a wide range of compositions can be obtained from bacteria such as *Azotobacter vinelandii* and *Pseudomonas spp.*, or commercially from brown marine macroalgae (*Phaeophyceae*) (Draget et al., 2006; Gorin & Spencer, 1966; Govan et al., 1981). The formation of hydrogels occurs with the ionic crosslinks of the alginates, mainly facilitated by the G-blocks that are crosslinked by multivalent cations and form stable crosslinks with Ca^{2+}, Sr^{2+} and Ba^{2+} (Mørch et al., 2006a). Alginates are attractive in biomedical applications due to their compatibility with high cell viability and low toxicity and immunogenicity profile (Lee & Mooney, 2012).

Cellulose is another naturally occurring and ubiquitous polymer consisting of 1–4 linked β-D-glucose residues. Various preparations of cellulose such as fibers, fibrils and microcrystals can be isolated from sources ranging from plant-based sources such as wood and agricultural residues to algae. Cellulose can also be biosynthesized by bacteria or produced by ocean dwelling animals known as tunicates such as *Ciona intestinalis* (Klemm et al., 2011; Zhao & Li, 2014). These latter organisms acquired the capacity to produce cellulose through lateral gene transfer of a bacterial cellulose synthase gene at the base of the tunicate lineage (Sagane et al., 2010). Nanocelluloses prepared by mechanical treatments, typically involving shearing, are termed cellulose nanofibrils (CNF) (Dufresne, 2017). CNFs derived from tunicates have several qualities which make them interesting in comparison with those derived from plants and bacteria. Notably, they have high molecular weight, the highest degree of crystallinity known in nature, the most robust fibrils (highest aspect ratio and stiffness) and can be produced at very high

* Corresponding author.
E-mail address: berit.l.strand@ntnu.no (B.L. Strand).

https://doi.org/10.1016/j.carbpol.2022.119284
Received 29 October 2021; Received in revised form 11 February 2022; Accepted 21 February 2022
Available online 25 February 2022

purity in the absence of contaminating lignins and hemicelluloses (Zhao & Li, 2014).

The use of hydrogels incorporating CNF has garnered research interest within tissue engineering and regenerative medicine (Markstedt et al., 2015; Nguyen et al., 2017). Hydrogels have several characteristics that are similar to those of the extracellular matrix such as a high water content, and rapid diffusion of nutrients, oxygen, and waste products (Frampton et al., 2011). Within the field of 3D bioprinting, the rheological and the mechanical properties of the biomaterials are key both to printability, resolution and maintaining the desired shape of the constructs. Although alginate can be crosslinked to a gel and solidify a scaffold, it flows too quickly when printed alone, and thus yields low print fidelity (Markstedt et al., 2015). For this reason, it is useful to combine alginate with other materials, such as nanocellulose. Nanocellulose dispersions are highly shear thinning: They exhibit very high viscosities at close to zero shear rate, yet much lower viscosities at a high shear rate (Markstedt et al., 2015). In other words, a combination of CNF and alginate allows for a substrate that is readily extrudable, that retains its shape following extrusion and that allows for crosslinking to maintain a solid construct. Thus, it is a much used and commercially available bioink for 3D printing (Athukoralalage et al., 2019; Wang et al., 2020). Composite hydrogels of alginate and CNF have been used for tissue engineering applications such as cartilage reconstruction (Martínez Ávila et al., 2015) and in combination with conductive polymer for energy storage (Françon et al., 2020). Although composite hydrogels of alginate and CNF have recently been described, both regarding mechanical properties (Aarstad et al., 2017; Heggset et al., 2019) as well as in relevant applications (Markstedt et al., 2015), no studies have, to our knowledge, investigated the production of alginate/tunicate CNF composite beads and subsequent encapsulation of cells that would be relevant for both cell therapy and tissue engineering applications.

We hypothesize that spherical and stable tunicate CNF-alginate microbeads with a high number of viable cells can be produced by the optimization of the parameters for production and gelling ions.

2. Materials and methods

2.1. Polysaccharides

Alginates, UP-LVG and LF200S were obtained from Novamatrix (Sandvika, Norway) and FMC Biopolymer AS (Sandvika, Norway), respectively. The composition and the molecular weight of the alginate determined with ^{1}H NMR (Grasdalen, 1983; Grasdalen et al., 1979) and SEC-MALLS (Vold et al., 2006), respectively, are given in Table 1. Alginate was labelled with fluoresceinamine for visualization in confocal laser scanning microscopy (CLSM), as previously described (Strand et al., 2003). CNF (TUNICELL ETC) derived from *C. intestinalis* was obtained from Ocean TuniCell AS (Bergen, Norway), based on a modified pulping procedure (Klemm et al., 2011; Zhao & Li, 2014) and mechanical homogenization (Zhao et al., 2017). The CNF crystallinity measured by X-ray diffraction (XRD) was 89.07 ± 1.60%. CNF average fibril lengths and width were determined using atomic force microscopy (AFM) at 2518 ± 827 nm, and 8.55 ± 3.37 nm, respectively.

2.2. Preparation of microbeads

Microbeads of alginate (A) and of alginate/CNF (A/C) were produced with a custom-built electrostatic droplet generator (NTNU, Trondheim, Norway) operated at 6.15 to 7 kV. Alginate was extruded with a syringe pump (Graseby Medical Ltd., Watford, Hertfordshire, UK) at 10–15 mL/h, using a 0.35 mm nozzle (Staedtler Mars GmbH & Co. KG, Nuremburg, Germany). Microbeads were made from 1.8% (w/v) total polysaccharide dry weight content, exclusively from alginate (A) or different ratios of alginate and CNF (A/C). Stock solutions of 2.5% (w/v) alginate and cellulose were mixed in different ratios corresponding to their relative weight fractions in the final mixture (Table 2) and diluted to a final concentration of 1.8% (w/v). The polysaccharides were dispersed and diluted in 4.6% (w/v) mannitol (VWR International BVBA, Leuven, Belgium) to provide physiological osmolarity. The gelling solution contained 50 mM $CaCl_2$ (Sigma-Aldrich, St. Louis, MO, USA) and 1 mM $BaCl_2$ (Merck KGaA, Darmstadt, Germany), 1.64% (w/v) mannitol, 10 mM HEPES (PanReac AppliChem GmbH, Darmstadt, Germany) and was pH adjusted to 7.2–7.4. To measure the size stability of calcium crosslinked microbeads, the microbeads in Fig. 3A were produced without 1 mM $BaCl_2$. Following gelation, microbeads were rinsed to remove gelling solution and unreacted gelling ions using a 0.9% NaCl (VWR International BVBA, Leuven, Belgium), 2 mM $CaCl_2$ and 10 mM HEPES solution at pH 7.2–7.4.

2.3. Visualization and size stability

Brightfield images and size determination of microbeads were obtained with a Nikon Eclipse TS100 microscope with a CFI Plan Fluor 4×/0.13 Phl DL (Nikon, Tokyo, Japan, software NIS Elements v. 4.51, build 1145). To assess stability with regard to osmotic swelling, microbeads were subjected to successive treatments in saline. Aliquots of 0.5 mL of microbeads were exposed to 3 mL of 0.9% NaCl solution for 1 h on a tube rotator. Images were captured and the saline solution was exchanged for repeated saline treatments.

2.4. Confocal imaging of fluorescent microbeads

Confocal Laser Scanning Microscopy (CLSM) was performed on microbeads produced from fluorescently labelled alginate (LF200S) and CNF. The fluorescent labelling of alginate with fluoresceinamine using carbodiimide chemistry has previously been described by Strand et al. (2003) (Strand et al., 2003). Images of equatorial sections (30 μm) were captured with an inverted confocal laser scanning microscope Zeiss LSM800 (Carl Zeiss AG, Jena, Germany) with a motorized XY-stage, and a C-apochromat 10× water-immersion objective (NA 0.45, WD 1.8 mm).

2.5. Gel stiffness and syneresis

The same polysaccharide and gelling solutions described in the "polysaccharides" and "production of microbeads" sections, were used to produce gel cylinders of alginate, and alginate/CNF. Gel cylinders were made by diffusion crosslinking (Skjåk-Bræk et al., 1989). Solutions of alginate and alginate/CNF were extruded into cylindrical casts and weighed. The cylindrical casts were enclosed in semipermeable membranes (Spectrum Laboratories, Inc., Rancho Dominguez, CA, USA). The casts with alginate and alginate/CNF were placed in gelling baths for 24 h. Following gelation, the gels were weighed and compressed. A Stable Micro Systems TA.XTplusC texture analyzer (Godalming, Surrey, UK), a P/35 cylindrical probe and a 5 kg load cell were used for compression. The compression was uniaxial and conducted at a probe speed of 0.1 mm/s with a trigger force of 1 g, at a temperature of 22 °C. Exponent

Table 1
Chemical composition of alginates given as fractions of G (F_G) and M (F_M), duplets (F_{GG}, F_{MM}, $F_{MG/GM}$) and triplets ($F_{GGM/MGG}$, F_{MGM}, F_{GGG}), estimates of G-block length ($N_{G>1}$) and weight average molecular weights (Mw). * LF200S was used exclusively as fluorescently labelled alginate for CLSM.

Alginate	F_G	F_M	F_{GG}	F_{MM}	$F_{MG/GM}$	$F_{GGM/MGG}$	F_{MGM}	F_{GGG}	$N_{G>1}$	Mw (kDa)
UP-LVG	0.68	0.32	0.57	0.21	0.11	0.04	0.07	0.53	16	237
LF200S*	0.68	0.32	0.57	0.21	0.11	0.04	0.08	0.53	14	298

Table 2
Microbead nomenclature, alginate (A, UP-LVG) and cellulose nanofibril (C, TUNICELL ETC) constituents with corresponding percentages of the total polymer content, and the corresponding alginate and cellulose nanofibril concentrations (w/v).

Microbead	Material(s), percentage of polymer in microbead	Concentration % (w/v)
A (100)	UP-LVG (100%)	1.80
A/C (80/20)	UP-LVG (80%)/TUNICELL ETC (20%)	1.44/0.36
A/C (50/50)	UP-LVG (50%)/TUNICELL ETC (50%)	0.90/0.90
A/C (40/60)	UP-LVG (40%)/TUNICELL ETC (60%)	0.72/1.08
A/C (30/70)	UP-LVG (30%)/TUNICELL ETC (70%)	0.54/1.26
A/C (20/80)	UP-LVG (20%)/TUNICELL ETC (80%)	0.36/1.44

Connect software v. 7.0.3.0 (Hamilton, MA, USA) was used for data collection and processing. Young's modulus (E) was calculated using the initial slope of the force-deformation curves, with correction for syneresis (Martinsen et al., 1989; Smidsrød et al., 1972) using the following equations:

$$E = S \times \left(\frac{L}{A}\right)$$

$$E\ Corr. = \frac{E}{\left(\frac{W_0}{W_1}\right)^2}$$

In which E is Young's modulus (Pa), L and A are the length (m) and area (m^2) of cylinders, and W_0 and W_1, respectively, are the masses (g) of each sample prior to and following gelation.

2.6. Rheology

The shear viscosities of alginate, alginate/CNF and CNF were analyzed using a TA Instruments Discovery HR-2 rheometer (Godalming, Surrey, UK). An aluminum plate-plate (20 mm, gap = 500 μm) was used and a Peltier plate with a temperature of 25 °C. The samples were allowed to reach equilibrium temperature for 60 s prior to each measurement. Shear viscosity was evaluated by increasing the shear rate from 0.1 to 1000 s^{-1}.

2.7. Permeability

Diffusion of macromolecules was investigated with 40, 70 and 150 kDa FITC-conjugated dextrans (Sigma-Aldrich, St. Louis, MO, USA) and absorbance spectrophotometry (VWR V1200, VWR International BVBA, Leuven, Belgium) at 490 nm. Aliquots of 2 mL of microbeads were incubated for 24 h at room temperature in 2 mL of 0.35% (w/v) dextran. The dextran solution was removed and five to six samples of 250 mg of microbeads were weighed. The microbeads were briefly rinsed in 1 mL of PBS (Medicago, Uppsala, Sweden) and the absorbance was measured. Three samples of microbeads were incubated in 1 mL PBS at room temperature on a rotator. Absorbance in the solution was measured immediately after incubation and at 15-minute intervals for 60 min. To determine the initial concentration of FITC dextran following the rinse, two to three samples of microbeads were dissolved in 1 mL of 0.15 M EDTA (VWR International BVBA, Leuven, Belgium) and filtered to provide a non-turbid solution. Identical microbeads were dissolved, filtered, and used as the blank sample.

2.8. Cells

In cell experiments, a pre-osteoblast cell line (MC3T3-E1 subclone 4, ATCC® CRL-2593™) from *Mus musculus*, strain (C57BL/6) calvaria was used. Additionally, Normal Human Dermal Fibroblasts (NHDFs), primary cells derived from adult skin were used (Lonza, Basel, Switzerland). NHDFs were cultured in FBM™ supplemented with FGM™-2 Fibroblast SingleQuots™ Kit (Lonza, Basel, Switzerland). MC3T3 cells were cultured in ascorbic acid free α-MEM (ThermoFisher Scientific, USA) supplemented with 1 μg/ml gentamicin, 2 mM glutamine and 10 % fetal calf serum (all supplements were from Sigma-Aldrich, St. Louis, MO, USA). Cells were sub-cultivated according to the manufacturer's recommendations.

2.9. Encapsulation

Cells were mixed with alginate and alginate/CNF to a final concentration of 1×10^6 cells/mL in 1.8% (w/v) polymer. Encapsulation of cells was performed by electrostatic droplet production (EDP), as described above (see section "Production of microbeads"). For cell encapsulation, cell suspensions require mixing with polymer solutions as well as extrusion (Fig. 1). Therefore, mixing and effects of extrusion on cell viability were investigated. For alginate/CNF microbeads two modes of mixing were tested: Stirring cell suspension into alginate and CNF with a spatula (Fig. 1A), and by a cell mixing device (CellInk, Boston, MA, USA) (Fig. 1B). Mixing was performed gently for approximately 1 min in both approaches. To investigate the impact of microbead production, some microbeads were gently extruded with a pipette (Fig. 1C) for comparison with EDP (Fig. 1D). Following encapsulation, microbeads and structures were gelled for 10 min before rinsing off excess gelling solution in Dulbecco's Modified Eagle's Medium (DMEM, Sigma-Aldrich, St. Louis, MO, USA). Encapsulated cells were transferred into growth medium and cell viability was assessed as described below.

2.10. Cell viability

Encapsulated cells were transferred into 150 μL of serum-free growth medium containing 1 μM DRAQ5 (Sigma-Aldrich, St. Louis, MO, USA) and 4 μM Ethidium homodimer-1 (EthD-1, ThermoFisher Scientific, USA) and incubated at room temperature for 30 min, to stain all (live and dead) and only dead cells, respectively. Imaging was performed on a Zeiss LSM800, as previously described (see section "Confocal imaging of fluorescent microbeads"). To determine cell viability, image acquisition was performed in triplicates with Z-projections of 50 stacks in 4.49 μm intervals. Quantitative analysis of the images obtained was carried out using ImageJ software (NIH). Differences between groups were compared applying a two-tailed *t*-test (Microsoft Office Excel 365). The significance level was set at 0.05. The results are expressed as mean ± standard deviation (SD).

3. Results

3.1. Shape and size of microbeads of alginate and CNF

Microbeads of alginate and of various alginate/CNF (A/C) ratios were prepared using an electrostatic droplet generator, to produce spherical beads of around 500 μm within a narrow size distribution, compatible with high cell viablity upon encapsulation. The beads were stabilized using barium in the gelling solution and characterised for permeablity of dextrans with different molecular weight. Microbead

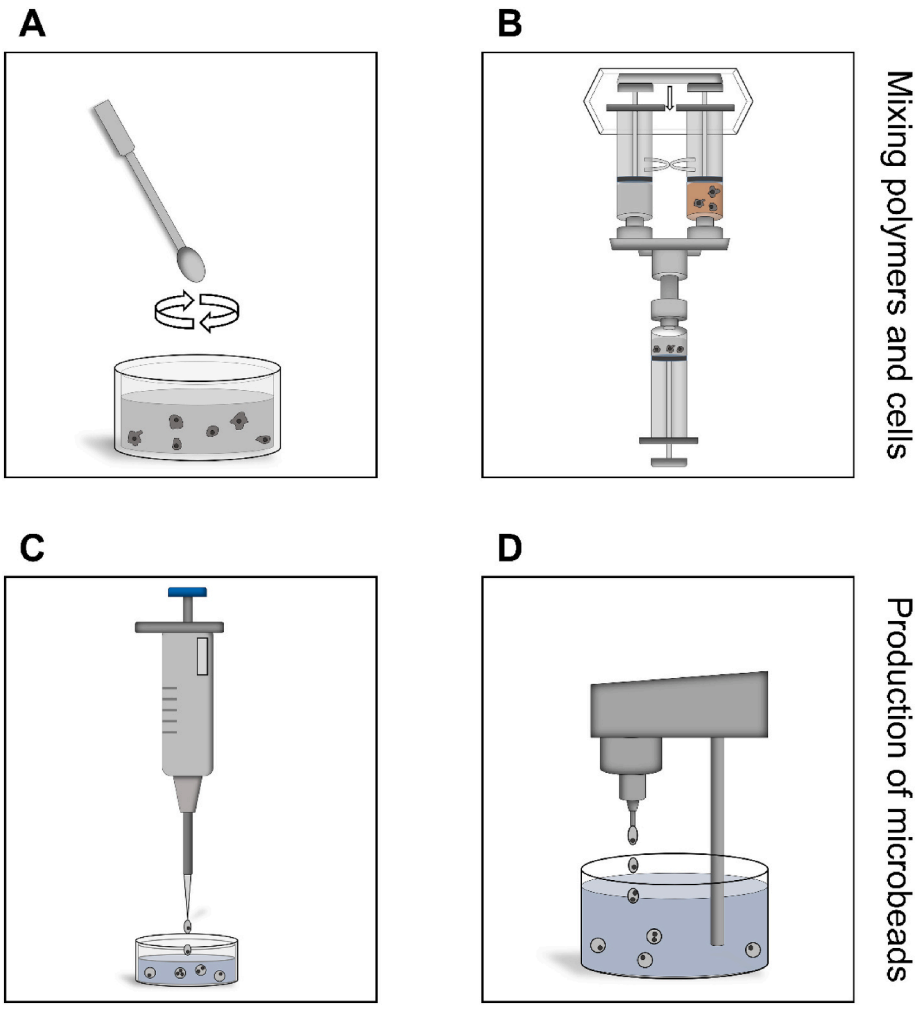

Fig. 1. Encapsulation of cells in alginate and alginate/CNF microbeads. **(A)** Mixing CNF and alginate with cell suspension using a spatula. **(B)** Mixing of alginate and CNF with cell suspension using a cell-mixing device. **(C)** Encapsulation by extrusion of microbeads using a pipette. **(D)** Encapsulation by electrostatic droplet production.

preparation was initially evaluated with different solutions at the same operating parameters (Fig. 2A), using a voltage of 7.00 kV, a flow rate of 10 mL/h and a nozzle diameter of 0.35 mm. During electrostatic microbead production, solutions with greater fractions of CNF appeared to increasingly elongate during extrusion. The maxima of elongation, and the resulting microbeads are depicted in Fig. 2A. More spherical composite microbeads with high CNF content (A/C (30/70) and A/C (20/80)) were produced at a reduced voltage (from 7.00 kV to 6.15 kV) and an increased flow rate (from 10 to 15 mL/h). Fig. 2B shows microbead size, size distribution, and the degree of elongation denoted as the aspect ratio for microbeads A/C (30/70) and A/C (20/80) produced using the new parameters (6.15 kV and 15 mL/h). The lower CNF content beads (60% CNF and below) where still produced with 7.00 kV and 10 mL/h. Fig. 2D shows representative pictures of the produced microbeads. Overall, the addition of CNF tended to increase size, size distribution and elongated microbeads (Fig. 2B): Microbeads with 50% CNF content or less had diameters of 449 ± 18 μm for A (100), 505 ± 13 μm for A/C (80/20) and 457 ± 37 μm for A/C (50/50) with aspect ratios of 1.05 ± 0.03, 1.06 ± 0.06, and 1.11 ± 0.07, respectively. Above 50% CNF, microbeads had greater diameters of 585 ± 78 μm for A/C (40/60), 542 ± 86 μm for A/C (30/70) and 601 ± 131 μm for A/C (20/80) with aspect ratios of 1.16 ± 0.18, 1.28 ± 0.17, and 1.23 ± 0.20, respectively. The microbeads with high CNF content (80% CNF) had both greater dispersity in size and aspect ratio (Fig. 2B), with some batch-to-batch variability (Fig. S1). A reduced total polymer concentration of 1.5% (w/v) produced results comparable to 1.8% (w/v) while an increase to 2.0% (w/v) led to higher aspect ratios, and size and dispersity (Fig. S1). To investigate the viscosity of alginate, CNF and alginate/CNF dispersions at different shear rates, a frequency sweep was performed (Fig. 2C), showing that the addition of CNF into alginate solution results in non-Newtonian and high shear thinning flow characteristics compared with alginate alone. CNF alone (C (100)) consistently produced the highest viscosity at any shear rate. At low shear rates, higher CNF content yielded substantially higher viscosity: Approximately 500-fold greater for A/C (20/80) compared to A (100) at 0.1 S^{-1}. The difference in viscosity decreased at higher shear rates, roughly overlapping (0.53–0.57 Pa·s) at 250 S^{-1} for A (100), A/C (50/50) and A/C (80/20).

3.2. Stability of alginate and alginate/CNF microbeads

To assess stability, A and A/C microbeads gelled with Ca^{2+} (50 mM) or with Ca^{2+}/Ba^{2+} (50 mM/1 mM) were subjected to successive saline treatments (0.9% (w/v) NaCl). Calcium crosslinked microbeads (50 mM, Fig. 3A) dissolved during the saline treatments. Increasing CNF content reduced the stability of the beads where A/C (80/20) dissolved after four treatments, A/C (50/50) after two treatments and A/C (20/80) after the first treatment, in contrast to the Ca-alginate microbeads A (100) dissolving after five treatments. Addition of 1 mM Barium ions to the gelling solution resulted in stable microbeads that did not dissolve during

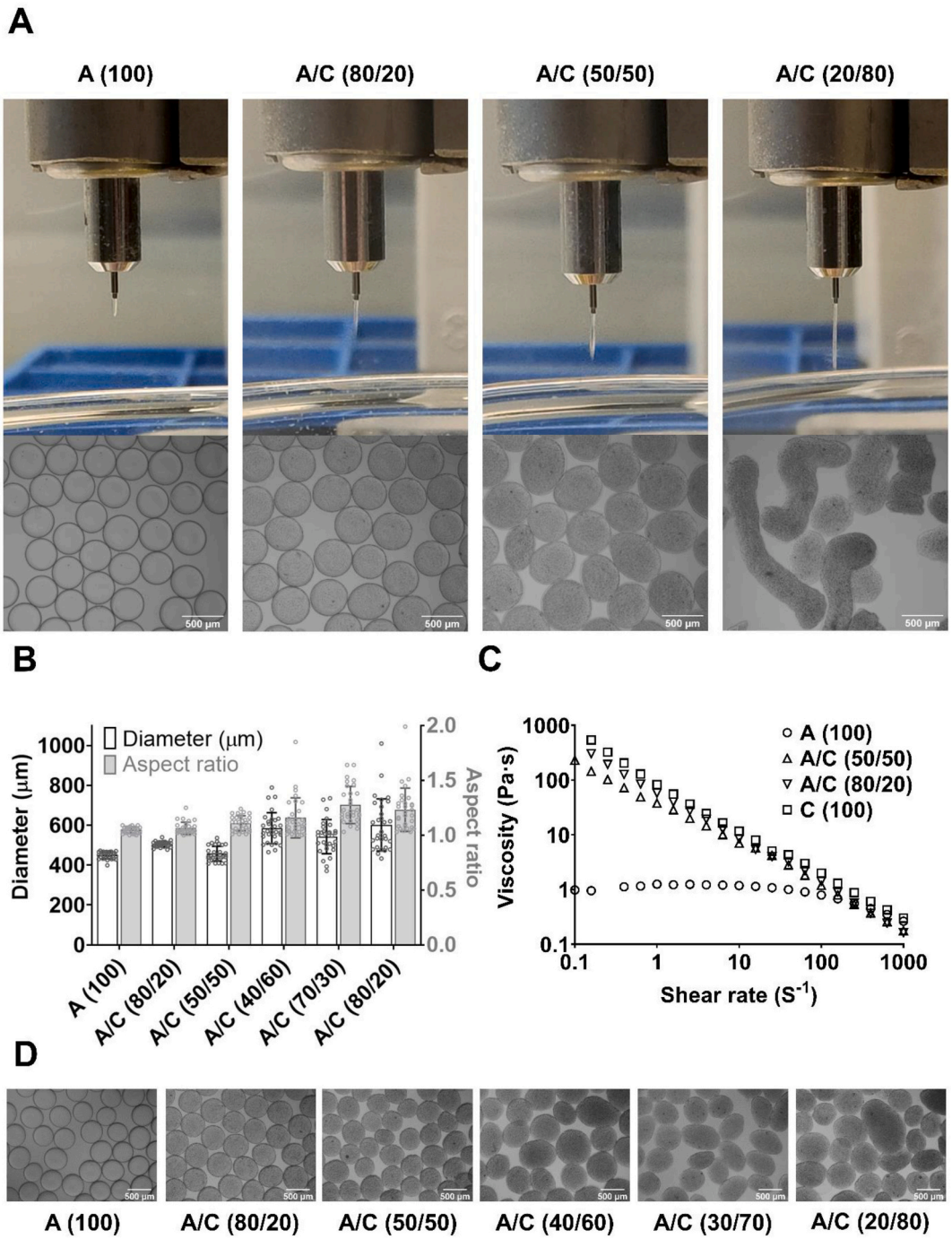

Fig. 2. Alginate and alginate/CNF (A/C) composite materials (1.8% (w/v) total polymer concentration). **(A)** Electrostatic droplet production with equal operating parameters (7 kV, 10 mL/h). The maxima of elongation of polymer solutions from the nozzle and resulting microbeads shown. Scale bar, 500 µm. **(B)** Diameters (left) and aspect ratios (right) of microbeads produced at 7.00 kV and 10 mL/h for A (100), A/C (20/80), A/C (50/50) and A/C (40/60) and 6.15 kV, 15 mL/h for A/C (30/70) and A/C (20/80). Diameters and aspect ratios are given as the mean ± SDEV, and scatter dots of individual values (n = 30). **(C)** Shear viscosity of 1.8% (w/v) polymer solutions in 4.6% (w/v) mannitol. **(D)** Representative images of microbeads used for measurements of diameter and aspect ratio in (B). A (100): Alginate, A/C (80/20): Alginate and CNF in 80/20 ratio, A/C (50/50): Alginate and CNF in 50/50 ratio, A/C (40/60): Alginate and CNF in 40/60 ratio, A/C (30/70): Alginate and CNF in 30/70 ratio, A/C (20/80): Alginate and CNF in 20/80 ratio, C (100): CNF. Scale bar, 500 µm.

the saline treatments (Fig. 3B). Furthermore, calcium/barium crosslinked microbeads exhibited substantially greater size stability through the saline treatments (Fig. 3B). CLSM images of equatorial sections of alginate and alginate/CNF microbeads gelled in Ca^{2+}/Ba^{2+} (50/1 mM), produced with fluorescently labelled alginate are shown in Fig. 3B. A slightly inhomogeneous distribution of alginate with greater signal from the fluorescent alginate towards the rim of the microbeads was observed for A (100) and A/C (80/20), but not for A/C (50/50). Due to limitations in transmission of light through A/C (20/80) microbeads, these microbeads were not visualized.

3.3. Stiffness of Ca/Ba-crosslinked alginate and alginate/CNF gels

To assess the stiffness of the Ca/Ba-crosslinked alginate/CNF composite gels, gel cylinders were chosen to reduce the complexity in measuring Young's modulus on microbeads due to changes of contact

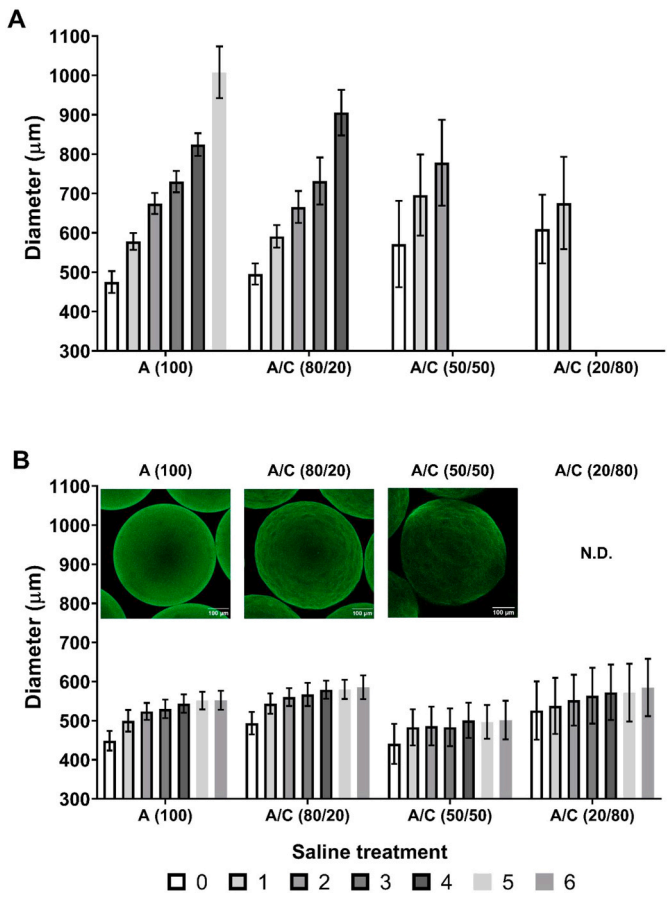

Fig. 3. Size increase of alginate and alginate/CNF microbeads in saline treatments (0.9% NaCl). **(A)** Microbeads gelled in Ca^{2+} (50 mM) and **(B)** Ca^{2+}/Ba^{2+} (50 mM/1 mM) and images of equatorial section (30 µm) by CLSM. Scale bar, 100 µm. Microbead diameters are given as the mean ± SDEV (n = 30). A (100): Alginate, A/C (80/20): Alginate and CNF in 80/20 ratio, A/C (50/50): Alginate and CNF in 50/50 ratio, A/C (80/20): Alginate and CNF in 80/20 ratio.

area upon uniaxial compression. Keeping the total polymer concentration constant (1.8% (w/v)), Young's modulus decreased with increasing content of CNF (Fig. 4A), with A (100) showing the highest (62.0 ± 9.6 kPa), A/C (50/50) slightly lower (55.4 ± 2.9 kPa) and A/C (20/80) showing the lowest (27.6 ± 2.9 kPa) modulus. Syneresis (release of water) was measured as the reduced weight of the material following gelation. Increased content of CNF largely reduced the syneresis of the hydrogels (Fig. 4B) with A (100) displaying the greatest syneresis (10.3 ± 0.8%), followed by A/C (50/50) (6.4 ± 2.2%) and lastly A/C (20/80) (1.3 ± 0.7%).

3.4. Permeability of Ca/Ba crosslinked alginate and alginate/CNF microbeads

Initial uptake and subsequent release of dextrans from microbeads was studied using FITC-conjugated dextrans and spectrophotometry. Uptake of 40 kDa dextran was comparable for A (100) (0.089 ± 0.007% (w/v)) and A/C (50/50) (0.088 ± 0.001% (w/v)). Uptake of 70 kDa dextran was slightly higher in the composite beads (A/C (50/50): 0.084 ± 0.001% (w/v)) as was 150 kDa dextran (0.070 ± 0.009% (w/v)) compared to microbeads with alginate alone (A (100): 70 kDa dextran = 0.070 ± 0.008%, and 150 kDa dextran = 0.061 ± 0.020% (w/v)). All sizes of dextrans released rapidly from all microbeads with the greatest fraction of release up to 15 min for both microbead types (Fig. 5D-F). A slightly higher initial (t = 0) release of 40 kDa dextran was seen for A/C (50/50) compared to A (100) (Fig. 5 D). The rate of release of 70 kDa dextran was slightly higher overall for A/C (50/50) than for A (100) (Fig. 5E), while release rates of 150 kDa were similar for both microbead types (Fig. 5F).

3.5. Cell encapsulation in Ca/Ba-crosslinked composite microbeads

Cell viability in microbeads A (100) and A/C (50/50) was studied using two cell types, the cell line MC3T3 and NHDF cells (Fig. 6A/C). Shortly after encapsulation the viability of MC3T3 cells was slightly greater (89.6 ± 2.6%) in A (100) than in A/C (50/50) microbeads (83.6 ± 0.4%). The viability of NHDFs in the A (100) microbeads was significantly ($p < 0.05$) higher (83.8 ± 5.0%.) than in the A/C (50/50) microbeads (66.2 ± 5.3%). Production and handling throughout the process of encapsulation may affect cell viability. Thus, the more sensitive NHDFs were chosen for evaluation of cell viability in A/C (50/50) microbeads produced with different techniques of mixing: Either gentle stirring with a spatula (Stir), or a cell-mixing device (Mixer), and different approaches for encapsulation: either by extrusion with a pipette (Pip.), or electrostatic droplet production (EDP) (Fig. 6B). In summary, the mixing of polymers and cells had a greater impact on cell viability than the production of microbeads. Mixing cells and polymers

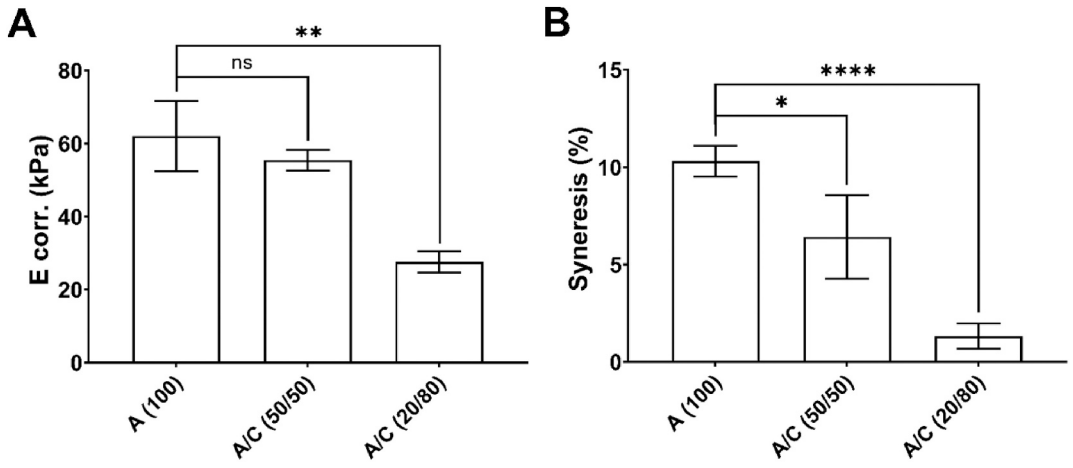

Fig. 4. Young's modulus and syneresis in gel cylinders of alginate (A 100), alginate/CNF (A/C 50/50) and A/C (20/80) gelled with Ca^{2+}/Ba^{2+} (50 mM/1 mM). **(A)** Young's modulus (E) corrected for syneresis, and **(B)** Syneresis. Measurements are given as the mean ± SDEV (N = 4). Statistically significant differences are indicated by * ($p < 0.05$), ** ($p < 0.01$) and **** ($p < 0.0001$). Alginate, A/C (80/20): Alginate and CNF in 80/20 ratio, A/C (50/50): Alginate and CNF in 50/50 ratio, A/C (80/20): Alginate and CNF in 80/20 ratio.

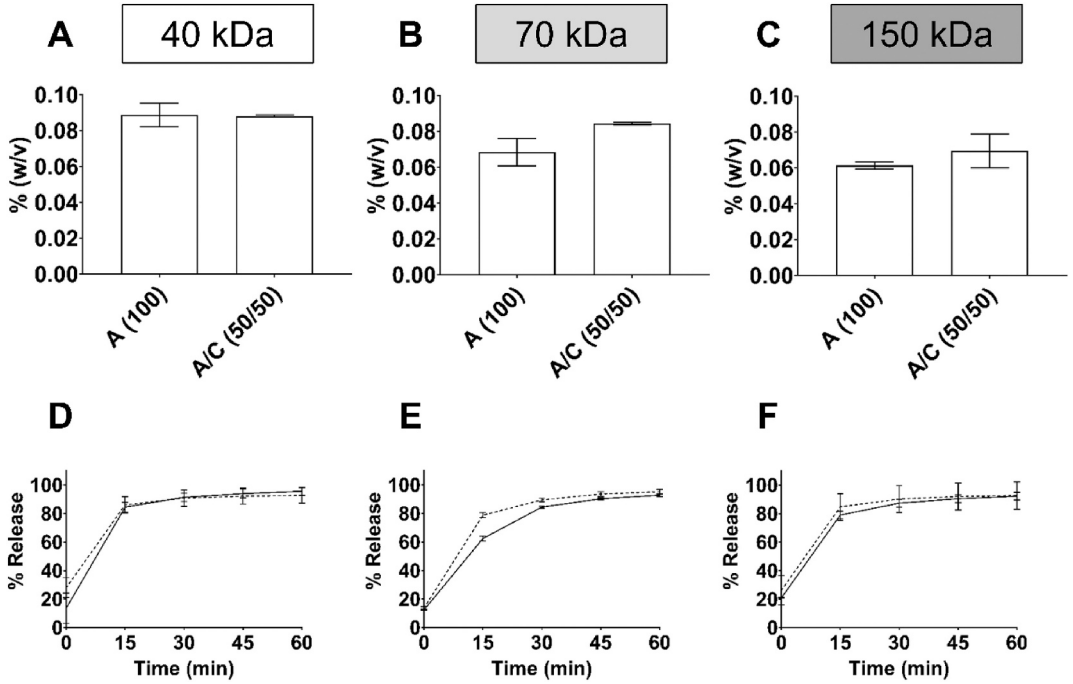

Fig. 5. Uptake and release of FITC-dextrans (40, 70 and 150 kDa), from microbeads A (100) and A/C (50/50). **(A–C)** Initial concentration (% (w/v)) of dextrans in microbeads **(D–F)** Percent release as a function of time where microbead A (100) is indicated by a solid line (—) and microbead A/C (50/50) is indicated by a dotted line (—). Measurements are given as the mean ± SDEV (N = 3, 2 in A).

by stirring with a spatula (Stir) yielded lower viability than the purpose-built cell-mixing device (Mixer). Production of microbeads with a pipette (Pip.) yielded slightly lower viability than microbeads produced by electrostatic droplet production (EDP) (Fig. 6B). NHDF viability in A/C (50/50) microbeads was lowest (51.3 ± 3.4%) for microbeads prepared by mixing cells and polymers by stirring with a spatula followed by pipette extrusion (Stir + Pip.). Viability was slightly higher (54.5 ± 3.7%) when microbeads were produced electrostatically (Stir + EDP).

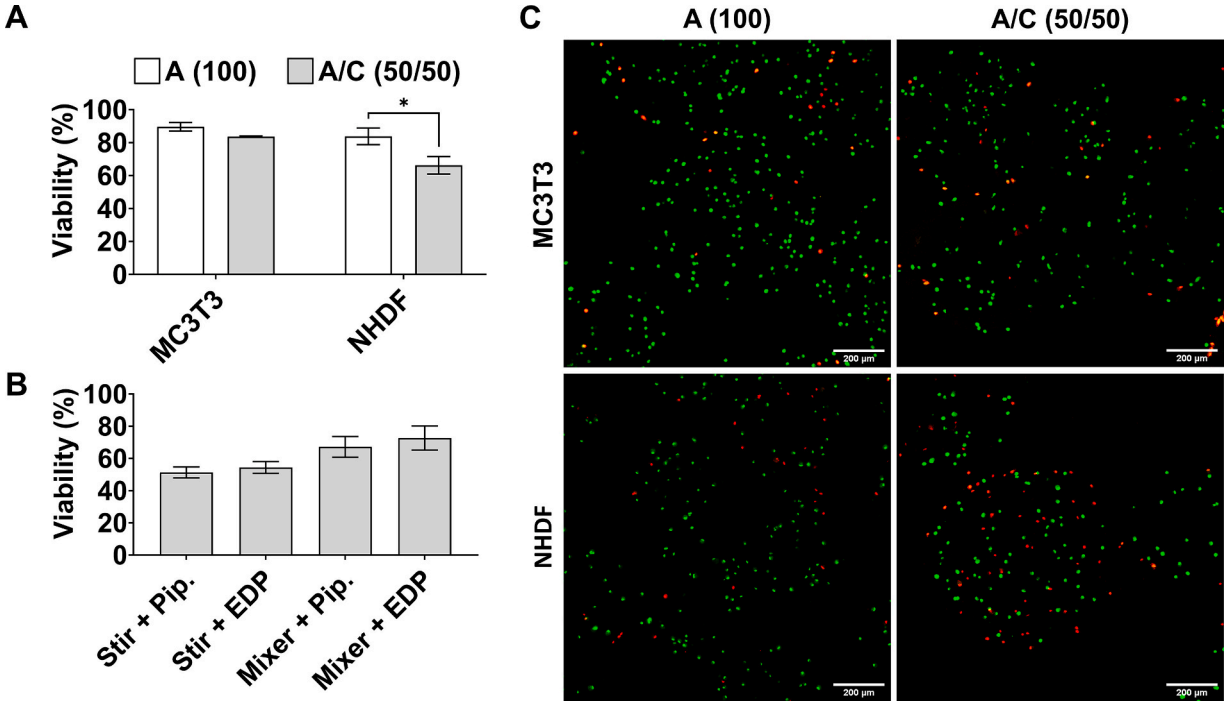

Fig. 6. Viability of cells after encapsulation. **(A)** MC3T3 and NHDF cells in A (100), mixed directly in a syringe, and A/C (50/50) mixed with cell-mixer: mean ± SDEV, statistically significant differences are indicated by * ($p < 0.05$, n = 2–4). **(B)** NHDF viability as a function of methods for cell-polymer mixing and extrusion. Cells were mixed with an A/C (50/50) polymer solution by stirring with a spatula (Stir) or a cell-mixing unit (Mixer). Microbeads were prepared dropwise by a pipetting (Pip.) or by electrostatic droplet production (EDP); mean ± SDEV (n = 2). **(C)** Z-projections of NHDFs and MC3T3s in microbeads. Scale bar, 200 µm. Dead cells are shown in red (EthD-1), and both live and dead cells are green (DRAQ5). Viability was measured on the same day as encapsulation (A–C). (For interpretation of the references to colour in this figure legend, the reader is referred to the web version of this article.)

Mixing cells and polymers with the cell mixer followed by pipette extrusion (Mixer + Pip.) yielded slightly lower viability (67.2 ± 6.5%) than electrostatically produced (Mixer + EDP) microbeads (72.7 ± 7.5%).

4. Discussion

4.1. Production of alginate/CNF microbeads

Alginate together with nanofibrillated cellulose is a commonly used bioink in 3D-bioprinting. However, to our knowledge, the application of alginate/nanofibrillated cellulose for electrostatic production of microbeads has not been reported. Furthermore, the high crystallinity and purity of nanocellulose from tunicates represents a highly relevant material for biomedical applications. Here, alginate and alginate/CNF microbeads in the range of 400 to 600 μm were produced using an electrostatic droplet generator. When starting from a fixed total polymer concentration (1.8% (w/v)) known to be suitable for electrostatic production (Strand et al., 2002) of stable microbeads (Martinsen et al., 1989; Mørch et al., 2006a), spherical microbeads of even size and size distribution were produced with up to 50% CNF content. Increasing the content of CNF in the polymer mixture resulted in elongation during extrusion and generated microbeads with increased size, size dispersity, and higher aspect ratios. Comparable results were obtained with reduced total polymer concentration (1.5% (w/v)), with increasing elongations at higher polymer concentrations (2.0% (w/v)). The shear thinning effect of nanofibrillated cellulose is well known and was also demonstrated here for alginate mixed with nanocellulose from tunicates. Alginate solutions have previously been shown to demonstrate some shear thinning rheological properties, and have a greater loss modulus compared to storage modulus over a wide range of frequencies (Rezende et al., 2009). In general, nanocellulose dispersions demonstrate pronounced shear thinning effects, which are largely ascribed to the alignment of cellulose fibrils when they are subjected to shear forces (Hubbe et al., 2017). Greater elongation of the polymer solution upon extrusion was observed for higher fractions of CNF, resulting in microbeads exhibiting a greater aspect ratio, size, and size dispersity, with some variation between batches. Considering the shear thinning properties demonstrated by CNF, the production of microbeads might be more sensitive to minor differences in the operational setup and thus the flow. Hence, while the shear thinning properties of CNF are ideal for printing as well as for production of microbeads up to a certain content of CNF as shown here, this may be the limiting factor for proper droplet production and shape recovery for microbead production using the electrostatic droplet generator.

4.2. Stability of alginate and alginate/CNF microbeads

Constructs made from nanocellulose and alginate within tissue engineering often use calcium ions for crosslinking (Krontiras et al., 2015; Markstedt et al., 2015; Nguyen et al., 2017; Wu et al., 2018). However, crosslinking alginate microbeads with barium or strontium ions has previously been reported to produce highly stable microbeads compared to crosslinking with calcium (Mørch et al., 2006b). Here, microbeads containing increasing concentrations of CNF, crosslinked with calcium, dissolved after fewer incubations with saline solutions. All of the calcium/barium crosslinked microbeads remained intact through saline treatments and demonstrated greatly reduced swelling compared to calcium crosslinked microbeads. Alginate gels are susceptible to exchange with non-gelling ions or chelating compounds that lead to swelling, compromised gel strength and dissolution (Rokstad et al., 2014). Accordingly, stability is a concern for both *in vitro* and *in vivo* applications where constructs are required to maintain their structure over time. Although barium crosslinked alginate yields stable gels, it has been shown in a mouse model that high G alginate barium crosslinked (20 mM) microbeads (0.3 mL) exceed the tolerable intake of barium (Mørch et al., 2012). A high concentration of barium used for crosslinking thus raises concerns about toxicity for *in vivo* applications. However, a mixture of 50 mM Ca^{2+} with 1 mM Ba^{2+} lends itself to producing high G alginate gels of sufficiently high strength and stability to swelling, while minimizing exposure to barium (Mørch et al., 2006b; Mørch et al., 2012).

4.3. Elasticity of Ca/Ba-crosslinked alginate/CNF composite gels

Although possible, investigating mechanical properties in microscale beads entails considerable complexity in contrast to gel cylinders (Kim et al., 2010). In the present study, gel cylinders were prepared by diffusion of calcium (50 mM) and barium (1 mM) ions, to resemble the gelation of microbeads. Decreasing alginate and increasing the CNF concentration in the cylinders reduced both Young's modulus and syneresis. Previously, Aarstad et al. reported that the Young's moduli of internally gelled, calcium saturated (50 mM) alginate/CNF gel cylinders increased with increasing content (0.15–0.75% (w/v)) of cellulose (Aarstad et al., 2017). In contrast, the present study kept the total polymer concentration constant (1.8% (w/v)). Accordingly, the concentration of alginate was lowered when CNF was incorporated. Ionic crosslinking of alginate gels leads to a decrease in volume and weight when compared to the solutions used to produce them (syneresis). This effect is ascribed to the formation of junction zones, which are largely responsible for generating the elastic properties in the ensuing alginate hydrogel (Draget et al., 2001). Accordingly, the reduction in gel strength of mixed alginate/CNF gels shown here is most likely caused by the lower concentration of crosslinked material.

4.4. Permeability of Ca/Ba crosslinked alginate and alginate/CNF microbeads

Permeability is an important variable in drug delivery systems, both regarding loading and rates of release, and in constructs containing cells that rely on diffusion of nutrients and cell products. De Vos et al. suggest two main factors as relevant for quantification of permeability, namely the rate of diffusion and the molecular weight cut-off (de Vos et al., 2009). While both are linked to diffusion, molecular weight cut-off (MWCO) alone does not predict diffusion since hydrogels are generally non-uniform with respect to properties such as the size of pores and their distribution, and material density (de Vos et al., 2009). In this study, minor differences in the diffusion of dextrans (40–150 kDa) between alginate and alginate/CNF microbeads were seen. Following incubation, all microbeads contained FITC-dextrans with slightly higher initial concentrations for lower molecular weight dextrans. Alginate/CNF microbeads held slightly more high molecular weight dextrans following incubation and showed slightly faster release of dextrans compared to alginate microbeads. This suggests that the rate of transfer of nutrients and therapeutic products may be slightly increased by the addition of CNF in microbeads. Cells entrapped within constructs such as microbeads rely on diffusion of essential nutrients and oxygen through the biomaterial. Previously, it has been reported that alginate/CNF gels produce more porous structures than alginate alone (Siqueira et al., 2019). The results herein showing slightly greater permeability of alginate/CNF microbeads compared to alginate microbeads might be linked to the higher porosity of these gel networks, as previously reported. What defines a desirable level of permeability is subject to debate (Calafiore, 2018; Korsgren, 2017; Strand et al., 2017). Rokstad et al. propose that what might be considered favorable permeability is application dependent, whether the application be *in vivo* or *in vitro* (Rokstad et al., 2014). In the context of immune isolation, some studies have found simple alginate microbeads with limited permselectivity (*i.e.*, isolation against direct contact with immune cells) to be adequate for sustained cell function *in vivo* (Duvivier-Kali et al., 2001; Omer et al., 2003). On the other hand, some *in vitro* studies have shown improved cell viability in hydrogels tailored for greater permselectivity against

inflammatory cytokines (Lin et al., 2010; Su et al., 2010).

4.5. Cell encapsulation

In tissue engineering, some applications require the entrapment of cells such as in cell therapy. In the process of producing constructs for cell immobilization, cell viability is a concern. Initial cell viability is useful as an indicator of the tolerability of the selected approach. Therefore, we encapsulated the mouse osteoblast precursor cell line MC3T3 and primary normal human dermal fibroblasts (NHDFs) in alginate and alginate/CNF microbeads to evaluate immediate viability following production. Overall, viability was high for the cells after encapsulation in the alginate/CNF microbeads, albeit higher viability was seen for the MC3T3 cells than for the NHDF (90% *vs* 66%, respectively), and higher viability was seen in the alginate microbeads. Hence, the effect on viability of mixing cells with polymers and extrusion was also investigated for the NHDFs. With respect to the mixing of polymers with cells and the mode of extrusion for microbead production the greatest impact on viability (NHDFs) was observed in the mixing process.

The decrease in viability of pre-osteoblast MC3T3 cells in the present study is in agreement with previously published findings showing a process-dependent decrease in the initial viability (down to 86–88%) of MC3T3 cells (Ahn et al., 2012; Lee et al., 2015). However, in contrast to the present study, previous studies have shown higher viability of human dermal fibroblasts following bioprinting. Viability greater than 90% has been reported using different bioinks, based on type I collagen (Lee et al., 2009), gelatin-poly(ethylene glycol)–tyramine (Hong et al., 2019), ECM-like material (Rimann et al., 2016), or high viscosity bioink based on 2% (w/w) of plant-derived nanofibrillated cellulose mixed with 0.5% (w/w) alginate (Thayer et al., 2018). In the latter work, it was also shown that viability of dermal fibroblasts was highly dependent on the mixing procedure. While Thayer et al. reported human dermal fibroblast viability over 90% at optimal mixing regimens (mixing unit or mixing with a spatula for 30 and 60 s), viability dropped to 77.9 ± 14% after mixing cells and bioink with a spatula for longer than 90 s. Similarly, shear-stress induced cell damage has been reported for mouse L929 fibroblasts. The viability of these cells decreased in 3D-bioprinting from 96 % to 76 % for 4 kPa and 18 kPa shear stresses, respectively (Blaeser et al., 2016). These observations are in line with studies in 3D bioprinting that found increased printing pressure and shear stress to adversely affect cell viability (Koo & Kim, 2016; Nair et al., 2009; Shi et al., 2018). A more prominent decrease in cell viability in A/C mixtures as compared to A, found in our work, is in agreement with previous observations for bovine chondrocytes. Viability of bovine chondrocytes was found to be 81%, approximately 50%, and over 95% in 0.5% (w/w) alginate/1.36% (w/w) nanocellulose mix, 1% (w/w) alginate sulfate/1.36% (w/w) nanocellulose mix, and control cellulose-free alginates, respectively (Müller et al., 2017). Therefore, it is likely that the viability of the encapsulated cells in our study was dependent on the encapsulation material, the chosen method of production as well as the type of cell encapsulated, as previously reported for other cell types (Gungor-Ozkerim et al., 2018; Malda et al., 2013). We also showed a dependency on material and cell type. However, cell viability was more strongly affected by the mixing protocol than by extrusion and electrostatic droplet generation.

5. Conclusions

Here, we show that composite microbeads of alginate/tunicate CNF can be produced with a narrow size range using an electrostatic bead generator and the extrusion of composite material into a solution of divalent cations. At a constant total polymer concentration of 1.8% (w/v) a greater content of CNF in the microbeads was linked to elongation of the polymers during extrusion and thus greater size, size distribution and aspect ratio, making it difficult to produce spherical beads with 80% content of CNF. Ionic crosslinking using calcium alone resulted in beads with increasing content of CNF exhibiting reduced stability. However, the addition of a low concentration of barium ions largely stabilized the beads, even with a high CNF content. Compression of 1.8% (w/v) gel cylinders revealed that Young's modulus decreased when adding CNF into alginate, but syneresis was reduced. Spectrophotometry using FITC-dextrans revealed that initial uptake and release rates were slightly higher in microbeads with CNF compared to alginate alone, indicating a slightly higher porosity. High (≈90%) viability was obtained for MC3T3 cells encapsulated in microbeads of alginate and alginate/CNF. The viability following mixing and mode of extrusion was investigated in alginate/CNF microbeads with NHDFs. Mixing was found to have greater impact than extrusion and electrostatic bead generation, and 66% viability of NHFDs were obtained in alginate/CNF beads upon optimizing the mixing protocol. The current study thus shows that composite alginate and tunicate CNF microbeads can be produced with an electrostatic bead generator. Such beads can be used for the encapsulation of cells and hence have the potential for use in both cell therapy and tissue engineering applications.

Supplementary data to this article can be found online at https://doi.org/10.1016/j.carbpol.2022.119284.

CRediT authorship contribution statement

Joachim S. Kjesbu: Conceptualization, Methodology, Validation, Investigation, Writing – original draft, Writing – review & editing, Visualization. **Daria Zaytseva-Zotova:** Conceptualization, Methodology, Validation, Formal analysis, Investigation, Writing – original draft. **Sanna Sämfors:** Investigation, Writing – original draft. **Paul Gatenholm:** Conceptualization, Writing – review & editing, Supervision, Project administration. **Christofer Troedsson:** Conceptualization, Resources, Writing – review & editing. **Eric M. Thompson:** Conceptualization, Resources, Writing – review & editing. **Berit Løkensgard Strand:** Conceptualization, Methodology, Validation, Writing – review & editing, Supervision, Project administration, Funding acquisition.

Declaration of competing interest

The authors declare the following financial interests/personal relationships which may be considered as potential competing interests: Christofer Troedsson and Eric M. Thompson are both employed at Ocean TuniCell, which provided the tunicate nanocellulose preparations used in this study.

The remaining authors declare that the research was conducted in the absence of any commercial or financial relationships that could be construed as a potential conflict of interest.

Acknowledgements

Wenche I. Strand is acknowledged for performing ^{1}H NMR. Ann-Sissel T. Ulset is acknowledged for analysis of alginates using SEC-MALLS. Their work was performed at the Department of Biotechnology and Food Science at NTNU. MC3T3 cells were provided by Sarah Lehnert and Kristin Grendstad, Department of Physics, NTNU, Trondheim, Norway. The NHDF cells were kindly provided by SINTEF Industry, Department of Biotechnology and Nanomedicine, Trondheim, Norway,

Funding

The Research Council of Norway is acknowledged for funding of the projects NFR-NANO 3D TUNINK and NFR-IPN TUNIGUIDE.

References

Aarstad, O., et al. (2017). Mechanical properties of composite hydrogels of alginate and cellulose nanofibrils. *Polymers, 9*(8), 378.

Ahn, S., et al. (2012). Cells (MC3T3-E1)-laden alginate scaffolds fabricated by a modified solid-freeform fabrication process supplemented with an aerosol spraying. *Biomacromolecules, 13*(9), 2997–3003.

Athukoralalage, S. S., et al. (2019). 3D bioprinted nanocellulose-based hydrogels for tissue engineering applications: A brief review. *Polymers, 11*(5), 898.

Blaeser, A., et al. (2016). Controlling shear stress in 3D bioprinting is a key factor to balance printing resolution and stem cell integrity. *Advanced Healthcare Materials, 5*(3), 326–333.

Calafiore, R. (2018). Microencapsulation for cell therapy of type 1 diabetes mellitus: The interplay between common beliefs, prejudices and real progress. *Journal of diabetes investigation, 9*(2), 231–233.

Draget, K. I., et al. (2001). Effects of molecular weight and elastic segment flexibility on syneresis in Ca-alginate gels. *Food Hydrocolloids, 15*(4), 485–490.

Draget, K. I., et al. (2006). Alginates. In *Food polysaccharides and their applications* (pp. 289–334). CRC Press.

Dufresne, A. (2017). Cellulose nanomaterial reinforced polymer nanocomposites. *Current Opinion in Colloid & Interface Science, 29*, 1–8.

Duvivier-Kali, V. F., et al. (2001). Complete protection of islets against allorejection and autoimmunity by a simple barium-alginate membrane. *Diabetes, 50*(8), 1698–1705.

Frampton, J. P., et al. (2011). Fabrication and optimization of alginate hydrogel constructs for use in 3D neural cell culture. *Biomedical Materials, 6*(1), Article 015002.

Françon, H., et al. (2020). Ambient-dried, 3D-printable and electrically conducting cellulose nanofiber aerogels by inclusion of functional polymers. *Advanced Functional Materials, 30*(12), 1909383.

Gorin, P. A. J., & Spencer, J. F. T. (1966). Exocellular alginic acid from azotobacter vinelandii. *Canadian Journal of Chemistry, 44*(9), 993–998.

Govan, J. R., Fyfe, J. A., & Jarman, T. R. (1981). Isolation of alginate-producing mutants of Pseudomonas fluorescens, pseudomonas putida and Pseudomonas mendocina. *Journal of General Microbiology, 125*(1), 217–220.

Grasdalen, H. (1983). High-field, 1H-n.m.r. spectroscopy of alginate: sequential structure and linkage conformations. *Carbohydrate Research, 118*, 255–260.

Grasdalen, H., Larsen, B., & Smidsrød, O. (1979). A p.M.R. Study of the composition and sequence of uronate residues in alginates. *Carbohydrate Research, 68*(1), 23–31.

Gungor-Ozkerim, P. S., et al. (2018). Bioinks for 3D bioprinting: An overview. *Biomaterials Science, 6*(5), 915–946.

Heggset, E. B., et al. (2019). Viscoelastic properties of nanocellulose based inks for 3D printing and mechanical properties of CNF/alginate biocomposite gels. *Cellulose, 26*(1), 581–595.

Hong, S., et al. (2019). Coaxial bioprinting of cell-laden vascular constructs using a gelatin-tyramine bioink. *BiomaterialsScience, 7*.

Hubbe, M., et al. (2017). Rheology of nanocellulose-rich aqueous suspensions: A review. *BioResources, 12*, 9556–9661.

Kim, K., et al. (2010). Investigation of mechanical properties of soft hydrogel microcapsules in relation to protein delivery using a MEMS force sensor. *Journal of Biomedical Materials Research Part A, 92A*(1), 103–113.

Klemm, D., et al. (2011). Nanocelluloses: A new family of nature-based materials. *Angewandte Chemie International Edition, 50*(24), 5438–5466.

Koo, Y., & Kim, G. (2016). New strategy for enhancing in situ cell viability of cell-printing process via piezoelectric transducer-assisted three-dimensional printing. *Biofabrication, 8*(2), Article 025010.

Korsgren, O. (2017). Islet encapsulation: Physiological possibilities and limitations. *Diabetes, 66*(7), 1748–1754.

Krontiras, P., Gatenholm, P., & Hägg, D. A. (2015). Adipogenic differentiation of stem cells in three-dimensional porous bacterial nanocellulose scaffolds. *Journal of Biomedical Materials Research Part B: Applied Biomaterials, 103*(1), 195–203.

Lee, H. J., et al. (2015). A new approach for fabricating Collagen/ECM-based bioinks using preosteoblasts and human adipose stem cells. *Advanced Healthcare Materials, 4*(9), 1359–1368.

Lee, K. Y., & Mooney, D. J. (2012). Alginate: Properties and biomedical applications. *Progress in Polymer Science, 37*(1), 106–126.

Lee, W., et al. (2009). Multi-layered culture of human skin fibroblasts and keratinocytes through three-dimensional freeform fabrication. *Biomaterials, 30*(8), 1587–1595.

Lin, C.-C., et al. (2010). Regulating MCP-1 diffusion in affinity hydrogels for enhancing immuno-isolation. *Journal of controlled release : official journal of the Controlled Release Society, 142*(3), 384–391.

Malda, J., et al. (2013). 25th anniversary article: Engineering hydrogels for biofabrication. *Advanced Materials, 25*(36), 5011–5028.

Markstedt, K., et al. (2015). 3D bioprinting human chondrocytes with nanocellulose-alginate bioink for cartilage tissue engineering applications. *Biomacromolecules, 16*(5), 1489–1496.

Martínez Ávila, H., et al. (2015). Novel bilayer bacterial nanocellulose scaffold supports neocartilage formation in vitro and in vivo. *Biomaterials, 44*, 122–133.

Martinsen, A., Skjåk-Bræk, G., & Smidsrød, O. (1989). Alginate as immobilization material: I. Correlation between chemical and physical properties of alginate gel beads. *Biotechnology and Bioengineering, 33*(1), 79–89.

Mørch, Y. A., et al. (2006). Effect of Ca2+, Ba2+, and Sr2+ on alginate microbeads. *Biomacromolecules, 7*(5), 1471–1480.

Mørch, Y. A., et al. (2006). Effect of Ca2+, Ba2+, and Sr2+ on alginate microbeads. *Biomacromolecules, 7*(5), 1471–1480.

Mørch, Y. A., et al. (2012). Binding and leakage of barium in alginate microbeads. *Journal of Biomedical Materials Research. Part A, 100*(11), 2939–2947.

Müller, M., et al. (2017). Alginate sulfate-nanocellulose bioinks for cartilage bioprinting applications. *Annals of Biomedical Engineering, 45*(1), 210–223.

Nair, K., et al. (2009). Characterization of cell viability during bioprinting processes. *Biotechnology Journal, 4*(8), 1168–1177.

Nguyen, D., et al. (2017). Cartilage tissue engineering by the 3D bioprinting of iPS cells in a nanocellulose/alginate bioink. *Scientific Reports, 7*.

Omer, A., et al. (2003). Survival and maturation of microencapsulated porcine neonatal pancreatic cell clusters transplanted into immunocompetent diabetic mice. *Diabetes, 52*(1), 69–75.

Rezende, R. A., et al. (2009). Rheological behavior of alginate solutions for biomanufacturing. *Journal of Applied Polymer Science, 113*(6), 3866–3871.

Rimann, M., et al. (2016). Standardized 3D bioprinting of soft tissue models with human primary cells. *Journal of Laboratory Automation, 21*(4), 496–509.

Rokstad, A. M. A., et al. (2014). Advances in biocompatibility and physico-chemical characterization of microspheres for cell encapsulation. *Advanced Drug Delivery Reviews, 67–68*, 111–130.

Sagane, Y., et al. (2010). Functional specialization of cellulose synthase genes of prokaryotic origin in chordate larvaceans. *Development, 137*(9), 1483–1492.

Shi, J., et al. (2018). Shear stress analysis and its effects on cell viability and cell proliferation in drop-on-demand bioprinting. *Biomedical Physics & Engineering Express, 4*(4), Article 045028.

Siqueira, P., et al. (2019). Three-dimensional stable alginate-nanocellulose gels for biomedical applications: Towards tunable mechanical properties and cell growing. *Nanomaterials (Basel), 9*(1).

Skjåk-Bræk, G., Grasdalen, H., & Smidsrød, O. (1989). Inhomogeneous polysaccharide ionic gels. *Carbohydrate Polymers, 10*(1), 31–54.

Smidsrød, O. H., Arne, & Lian, B. (1972). Properties of poly(1,4-hexuronates) in the gel state. I. Evaluation of a method for the determination of stiffness. *Acta Chemica Scandinavia, 26*, 79–88.

Strand, B. L., et al. (2002). Alginate-polylysine-alginate microcapsules: Effect of size reduction on capsule properties. *Journal of Microencapsulation, 19*(5), 615–630.

Strand, B. L., et al. (2003). Visualization of alginate-poly-L-lysine-alginate microcapsules by confocal laser scanning microscopy. *Biotechnology and Bioengineering, 82*(4), 386–394.

Strand, B. L., Coron, A. E., & Skjåk-Bræk, G. (2017). Current and future perspectives on alginate encapsulated pancreatic islet. *Stem Cells Translational Medicine, 6*(4), 1053–1058.

Su, J., et al. (2010). Anti-inflammatory peptide-functionalized hydrogels for insulin-secreting cell encapsulation. *Biomaterials, 31*(2), 308–314.

Thayer, P. S., Orrhult, L. S., & Martínez, H. (2018). Bioprinting of cartilage and skin tissue analogs utilizing a novel passive mixing unit technique for bioink precellularization. *Journal of Visualized Experiments, 131*.

Vold, I. M. N., Kristiansen, K. A., & Christensen, B. E. (2006). A study of the chain stiffness and extension of alginates, in vitro epimerized alginates, and periodate-oxidized alginates using size-exclusion chromatography combined with light scattering and viscosity detectors. *Biomacromolecules, 7*(7), 2136–2146.

de Vos, P., et al. (2009). Multiscale requirements for bioencapsulation in medicine and biotechnology. *Biomaterials, 30*(13), 2559–2570.

Wang, X., Wang, Q., & Xu, C. (2020). Nanocellulose-based inks for 3D bioprinting: Key aspects in research development and challenging perspectives in applications-a mini review. *Bioengineering (Basel, Switzerland), 7*(2), 40.

Wu, Y., et al. (2018). 3D bioprinting of liver-mimetic construct with alginate/cellulose nanocrystal hybrid bioink. *Bioprinting, 9*, 1–6.

Zhao, Y., & Li, J. (2014). Excellent chemical and material cellulose from tunicates: Diversity in cellulose production yield and chemical and morphological structures from different tunicate species. *Cellulose, 21*(5), 3427–3441.

Zhao, Y., et al. (2017). Cellulose nanofibers from softwood, hardwood, and tunicate: Preparation–Structure–Film performance interrelation. *ACS Applied Materials & Interfaces, 9*(15), 13508–13519.